Fabrication of grain refiners with high volume fraction of $Al_{2.7}Fe_{0.3}Ti$ heterogeneous nucleation site particles by spark plasma sintering

Yoshimi Watanabe[1]*, Syusuke Taniai[1], and Hisashi Sato[1]

[1]*Department of Physical Science and Engineering, Graduate School of Engineering, Nagoya Institute of Technology, Nagoya 466-8555, Japan*

* E-mail: yoshimi@nitech.ac.jp

In our previous study, a novel Al-$L1_2$-type $Al_{2.7}Fe_{0.3}Ti$ refiner is fabricated by spark plasma sintering (SPS) and its refining performance was studied. It is found that $L1_2$-type $Al_{2.7}Fe_{0.3}Ti$ particles can be favorable heterogeneous nucleation sites for Al casts, since the lattice matching between $Al_{2.7}Fe_{0.3}Ti$ and Al is good. If the volume fraction of $Al_{2.7}Fe_{0.3}Ti$ heterogeneous nucleation site particles in the refiner is increased, the same amount of heterogeneous nucleation site particles can be added even if the addition amount of the grain refiner is decreased. Therefore, it can contribute to the reduction of the cost of the refiners. In this paper, Al-$Al_{2.7}Fe_{0.3}Ti$ refiners with high volume fraction of the $Al_{2.7}Fe_{0.3}Ti$ heterogeneous nucleation site particles are fabricated by SPS and investigated the effect on refining performance.

1. Introduction

As one of the methods for refining of the α-Al grains in as-cast Al, addition of refiners such as Al-Ti, Al-Ti-B and Al-Ti-C system alloys has been carried out. It is known that Al_3Ti, TiB_2, and TiC particles in the Al melt act as the heterogeneous nucleation sites. [1-6] According to classical nucleation theory, the formation of a stable nucleus depends on the competition between the driving force for the phase transformation from liquid to solid (the volume free energy) and the energy required for the formation of a new interface. As shown in Fig. 1, since the volume of spherical segment, V, surface area of spherical cap, A_C and basement area of spherical cap, A_B, are given as

$$V=1/3\ \pi h^2(3R-h),\quad h=R(1-\cos\theta) \tag{1}$$

$$Ac=2\pi Rh=2\pi R^2(1-\cos\theta) \tag{2}$$

$$A_B=\pi R^2\sin^2\theta \tag{3},$$

the free energy barrier for nucleation on a heterogeneous substrate, ΔG_{hetero}^{*}, can be described by [5,7]

$$\Delta G_{hetero}^{*}=\frac{16\pi(\gamma_{LC})^3T_M^2}{3L^2\Delta T^2}\left\{\frac{(2+\cos\theta)(1-\cos\theta)^2}{4}\right\} \tag{4}$$

where γ_{LC} is the interfacial free energy of the liquid/crystal interface, T_M is the equilibrium melting temperature, L is the latent heat of solidification, ΔT is the undercooling below the liquidus temperature and θ is the wetting angle between the liquid phase and the heterogeneous nucleation substrate. $16\ \pi\ (\gamma_{LC})^3\ T_M^2\ /\ 3L^2\Delta T^2$ in eq. (4) is free energy barrier for homogeneous nucleation. Figure 2 shows the $\{(2+\cos\theta)(1-\cos\theta)^2\}/4$ value as a function of wetting angle, θ. As can be seen, the free energy barrier for nucleation is decreased by decreasing the wetting angle of the heterogeneous substrate.

It is well accepted that an effective refiner contains heterogeneous nucleation sites having a smaller lattice mismatching with the metal matrix, *i.e.*, having a smaller wetting angle with the metal matrix. Some formulas are proposed to describe the lattice mismatching, including disregistry [8] and plane disregistry. [9] Kato has investigated the preferred epitaxial relationship (crystallographic orientation relationship) between the deposit and the substrate of metals using M, which is approximately proportional to the specific misfit strain energy. [10-12] The parameter M is defined as

$$M = \varepsilon_1^2 + \varepsilon_2^2 + (2/3)\ \varepsilon_1\ \varepsilon_2, \quad (5)$$

where ε_1 and ε_2 are the principal misfit strains calculated from the principal distortions. According to his study, the epitaxial relationship with small *M* values becomes the preferred one. Although this consideration has often been applied to epitaxial phenomena, it is potentially applicable to predicting the preferred orientation relationship between two solidified phases. [13] Therefore, choice of heterogeneous nucleation site with small *M* value is one of key issues to develop superior grain refiner.

In our previous studies, [14-17] it has been shown that $L1_2$ modified $(Al_{1-x}Me_x)_3Ti$ intermetallic compounds [18-21] show good grain refining performance, although $L1_2$ modified $(Al_{1-x}Me_x)_3Ti$ intermetallic compounds cannot coexist with Al matrix in an equilibrium state. Al-10vol%$Al_{2.7}Fe_{0.3}Ti$ and Al-10vol%$Al_{2.7}Ni_{0.3}Ti$ refiners with *M* values of 2.50×10^{-3} and 1.93×10^{-3} respectively are successfully fabricated by spark plasma sintering (SPS). [14-16] This is because SPS can be carried out at a low temperature with short heating, holding, and cooling times, [22-24] which can be achieved in a non-equilibrium state.

The grain refining performance of refiner could be also improved by decreasing the size of heterogeneous nucleation site particles and increasing in the number density of nucleation sites [25-27] by using severe plastic deformation (SPD) technique. [28-30] It is also found that cold rolled Al-Al_3Ti refiner shows enhanced grain refining performance. [31] If the refiner has double number of heterogeneous nucleation site particles, half amount of addition could show the same grain refining performance. This will result in the reducing of refiner cost of manufacturing. Recently grain refining performance of the refiners with high volume fraction of $Al_{2.5}Cu_{0.5}Ti$ heterogeneous nucleation site particles up to 40vol% was studied. [27] In the present study, refiners with high volume fraction of $Al_{2.7}Fe_{0.3}Ti$ heterogeneous nucleation site particles were, therefore, fabricated by SPS from mixed-powder of Al particles and $Al_{2.7}Fe_{0.3}Ti$ particles, to reduce the addition level of refiners into molten Al. Grain refining performance was, then, studied using fabricated refiners. Especially, mixing conditions of mixed-powder are focus to study the distribution of $Al_{2.7}Fe_{0.3}Ti$ particles in refiner on grain refinement performance.

2. Experimental methods

In this study, $Al_{2.7}Fe_{0.3}Ti$ particles having $L1_2$ structure were directly prepared by gas

atomization, as shown in Fig. 3(a). The atomization gas was Ar and its pressure was 4.5 MPa. The gas-atomized $Al_{2.7}Fe_{0.3}Ti$ particles were sieved in the range of 75-150 μm, as shown in Fig. 3(b). The sieved $Al_{2.7}Fe_{0.3}Ti$ particles were mixed with pure Al particles (99.9%, 106–180 μm), where the volume fractions of $Al_{2.7}Fe_{0.3}Ti$ particles were 5vol%, 10vol%, 20vol%, 30vol%, 40vol%, and 50vol %. A three-dimensional motion mixer (Turbula mixer), in which the container motion consists of two rotations of the container around its longitudinal axis and a horizontal translation, [32] was used to achieve uniform mixing of powder, as shown in Fig. 3(c). Mixing time was fixed to be 60 min except for 40vol% case. In case of 40vol% mixture, the mixing time was varied (10 min, 60 min, and 300 min) to examine the distribution of $Al_{2.7}Fe_{0.3}Ti$ particles in refiner on grain refinement performance. A process control agent, such as stearic acid (CH_3 $(CH_2)_{16}COOH$), is often added to the starting powder in order to minimize powder aggregation and cold-welding effects. [33,34] The effect of addition of stearic acid on the spatial distribution of $Al_{2.7}Fe_{0.3}Ti$ particles in refiner is also studied, where mixing time was 60 min.

The mixed powder was sintered by SPS apparatus (SPS Syntax SPS-515S) at 500 °C for 5 min under an applied stress of 45 MPa, as shown in Fig. 3(d). Microstructures of the fabricated refiners were studied by scanning electron microscope (SEM), an energy-dispersive X-ray spectrometry (EDS), and X-ray diffractometer (XRD). For the Al-40vol%$Al_{2.7}Fe_{0.3}Ti$ refiners fabricated under different mixing conditions, internal defect analysis by X-ray computer tomography (CT) and evaluation of spatial distribution of $Al_{2.7}Fe_{0.3}Ti$ particles by Morisita Index I_δ [35-37] were carried out. The X-ray CT measurements were carried out using micro focus X-Ray device (SHIMADZU, InspeXio SMX-225CT). From obtained sectioned files, 3-dimensional (3D) images showing the internal defects are reconstructed using VGStudio MAX 3.1 VerUP.

Casting experiments were conducted to investigate the refining performance of refiners with high volume fraction of $Al_{2.7}Fe_{0.3}Ti$ heterogeneous nucleation site particles. Commercially pure Al ingot (99.99% purity) was melted in an alumina crucible using the electrical resistance furnace at 750 °C in argon gas atmosphere. After the addition of the refiner into the melt, the melt was stirred with a rod for 30 s, after which no further stirring was carried out. The melt was cast into a cylindrical steel mold of 45mm in inner diameter, 70mm in outer diameter, and 70mm in height after a holding time of 0, 210, 390, 600, or

1200 s. Here, the holding time is the time interval from when the stirring was finished to when the melt was cast into the mold. The casting conditions are summarized in Table I. The Al castings were subjected to optical microscopy, and grain size analysis was carried out using the Mean Linear Intercept method after etching the polished surface with a 10% hydrofluoric acid aqueous solution.

3. Results and discussion

3.1 Microstructure of Al–$Al_{2.7}Fe_{0.3}Ti$ refiners

The microstructure of the fabricated refiners are shown in Figs. 4(a)-4(f). The magnified microstructures of these refiners are shown in Figs. 4(a')-4(f'), respectively. The results of the compositional analysis of the refiner in Figs. 4(a') by EDS are shown in Table II. It can be observed that matrix is almost pure Al, while a gray phase and white mesh-shaped phase found in gas-atomized particles are identified to be stoichiometric chemical composition of $Al_{2.7}Fe_{0.3}Ti$ and Fe-rich secondary phase, respectively. It is also found from Figs. 4(a')-4(f') that clear interface exists between Al matrix and $Al_{2.7}Fe_{0.3}Ti$ particles. The XRD patterns of these refiners are shown in Figs. 5(a)-5(f), respectively. It can be seen from Figs. 4 and Figs. 5 that the $Al_{2.7}Fe_{0.3}Ti$ particles with $L1_2$ structure are successfully dispersed in the Al matrix. From this, it is concluded that refiners containing high volume fraction of the $Al_{2.7}Fe_{0.3}Ti$ heterogeneous nucleation site particles were fabricated without any reaction by using SPS.

In cases of Al-40vol%$Al_{2.7}Fe_{0.3}Ti$ and Al-50vol%$Al_{2.7}Fe_{0.3}Ti$ refiners, however, aggregation of $Al_{2.7}Fe_{0.3}Ti$ particles was observed, and some pores can be found around the aggregated region. Densities of these refiners are measured by the Archimedes method, and the relative densities are shown in Table III. The density of the refiners decreases with increasing the volume fraction of $Al_{2.7}Fe_{0.3}Ti$ particles. The relative density of Al-40vol%$Al_{2.7}Fe_{0.3}Ti$ and Al-50vol%$Al_{2.7}Fe_{0.3}Ti$ refiners is about 2% lower than that of other refiners. This is because Al matrix does not spread into the aggregated portion of $Al_{2.7}Fe_{0.3}Ti$ particles.

3.2 Grain refinement performance of Al–$Al_{2.7}Fe_{0.3}Ti$ refiners

By using the fabricated refiners, the grain refinement performance is studied, and obtained macrostructures of the Al casts are shown in Figs. 6(a)-6(f), respectively. From left figures to right figures, the holding times are 0 s, 210 s, 390 s, 600 s, and 1200 s. For comparison, the macrograph of an unrefined pure Al cast is shown in Fig. 6(g). The unrefined pure Al cast is composed of very coarse columnar grains, and the mean grain size of the unrefined pure Al cast was 3212 μm. The addition of Al-5vol%$Al_{2.7}Fe_{0.3}Ti$, Al-10vol%$Al_{2.7}Fe_{0.3}Ti$, Al-20vol%$Al_{2.7}Fe_{0.3}Ti$, and Al-30vol%$Al_{2.7}Fe_{0.3}Ti$ refiners can markedly refine the Al cast. Complete conversion of coarse columnar grain structure to fine equiaxed grains occurred by addition of these refiners after holding time of 390 s. This is because the $L1_2$ modified $Al_{2.7}Fe_{0.3}Ti$ has smaller M value and smaller $\{(2+\cos\theta)(1-\cos\theta)^2\}/4$ value, show in Fig. 2, which indicate the free energy barrier for nucleation on $Al_{2.7}Fe_{0.3}Ti$ particle is small. However, the grain refining performances of the Al-40vol%$Al_{2.7}Fe_{0.3}Ti$ and Al-50vol%$Al_{2.7}Fe_{0.3}Ti$ refiners were different. The macrographs of Al casts refined by Al-40vol%$Al_{2.7}Fe_{0.3}Ti$ refiner present columnar grains as well as equiaxed grains. In case of the Al-50vol%$Al_{2.7}Fe_{0.3}Ti$ refiner, only weak grain refining performance is observed.

Figure 7 shows the average grain size of Al casts refined with the Al-$Al_{2.7}Fe_{0.3}Ti$ refiners plotted against the holding time. The refiners containing different amounts of heterogeneous nucleation site particles showed differences in the grain refining performance with the holding time, even though the total amount of $Al_{2.7}Fe_{0.3}Ti$ heterogeneous nucleation site particles within the melt was the same. Although the Al-5vol%$Al_{2.7}Fe_{0.3}Ti$, Al-10vol%$Al_{2.7}Fe_{0.3}Ti$, Al-20vol%$Al_{2.7}Fe_{0.3}Ti$, and Al-30vol%$Al_{2.7}Fe_{0.3}Ti$ refiners show similar grain refining performance, reduced grain refinement performance of refiners with high volume fraction of heterogeneous nucleation site particles was found. The finest grain size of casts refined by Al-5vol%$Al_{2.7}Fe_{0.3}Ti$, Al-10vol%$Al_{2.7}Fe_{0.3}Ti$, Al-20vol% $Al_{2.7}Fe_{0.3}Ti$, Al-30vol%$Al_{2.7}Fe_{0.3}Ti$, Al-40vol%$Al_{2.7}Fe_{0.3}Ti$, and Al-50vol%$Al_{2.7}Fe_{0.3}Ti$ refiners are 227 μm, 218 μm, 211 μm, 178 μm, 512 μm, and 929 μm, respectively. In case of Al-40vol%$Al_{2.7}Fe_{0.3}Ti$ refiner, the same amount of heterogeneous nucleation site particles can be added even if the addition amount of the grain refiner is one fourth of Al-10vol%$Al_{2.7}Fe_{0.3}Ti$ refiner. This will result in the reducing of cost of manufacturing. However, since pores and aggregated particles were existed in the Al-40vol%$Al_{2.7}Fe_{0.3}Ti$ refiner, reduced grain refinement performance was found. It is expected that the grain

refining performance could be enhanced by decreasing such pores and aggregated particles. Next, to improve their grain refining performance, the effects of mixing conditions on microstructure of Al-40vol% $Al_{2.7}Fe_{0.3}Ti$ refiners will be studied.

3.3 Effects of mixing conditions on microstructure of Al-40vol%$Al_{2.7}Fe_{0.3}Ti$ refiners

In this study, our final goal is fabricate grain refiners with high volume fraction of $Al_{2.7}Fe_{0.3}Ti$ heterogeneous nucleation particles. As mentioned the above, however, reduced grain refinement performance was found for the refiners containing the $Al_{2.7}Fe_{0.3}Ti$ particles more than 40vol%. The pores and aggregated particles observed in these refiners, which may influence the grain refinement performance, can be controlled by changing the mixing conditions, such as mixing time and addition of process control agent. The microstructures of the Al-40vol%$Al_{2.7}Fe_{0.3}Ti$ refiners fabricated under mixing time of 10 min, 60 min and 300 min without stearic acid, and 60 min with stearic acid are shown in Figs. 8(a)-8(d), respectively. It is seen that that significant influence of mixing time does not found on the microstructure of refiners with high volume fraction of heterogeneous nucleation site particles. It must be noted here, however, the addition of the stearic acid reduce the amount and size of pores. Since it is known that the stearic acid acts as the process control agent, [38,39] homogeneous distribution of $Al_{2.7}Fe_{0.3}Ti$ particles can be achieved by lubrication of stearic acid.

The density of each refiner was measured by the Archimedes method, and obtained relative density is listed in Table IV. The relative density of Al-40 vol%$Al_{2.7}Fe_{0.3}Ti$ refiner fabricated with the stearic acid is more than 96%, which is comparable with that of Al-30 vol%$Al_{2.7}Fe_{0.3}Ti$ refiner. Therefore, it is expected that the Al-40 vol%$Al_{2.7}Fe_{0.3}Ti$ refiner fabricated with the stearic acid shows better grain refining performance.

The spatial distribution of $Al_{2.7}Fe_{0.3}Ti$ particles in these refiners are evaluated using Morisita Index, I_δ. The I_δ has been proposed as a measure of dispersion of individuals in a population, [35-37] which can be used to analyse local versus global dispersions. The index value is computed as :

$$I_\delta = q \cdot \delta \tag{6}$$

$$\delta = \frac{\sum_{i-1}^{q} n_i(n_i-1)}{N(N-1)} \quad (7)$$

where n_i is the number of individuals in the i^{th} quadrat (i =1, 2, 3, ..., q), q is the number of quadrat, and N is given by

$$N = \sum_{i=1}^{q} n_i \quad (8).$$

The most important property of the I_δ is that it is uninfluenced by N provided that each sample unit is randomly taken from each of q groups into which an infinite population is divided with respective proportions. Utilizing this index, methods for analyzing the pattern of distribution of individuals and estimating the clump sizes on an area have also been developed. Thus, the I_δ divides the original image using different sizes of quadrat, and then based on the number of particles in each quadrat, a weighted index is calculated to represent the dispersion status of an image.

Typical particle distributions, Poisson's distribution, uniform distribution, and aggregated distribution are illustrated in Figs. 9(a), 9(b), and 9(c), respectively. For these distributions, I_δ are calculated and results are plotted against q as shown in Fig. 10. The Poisson's distribution has $I_\delta = 1$, while the uniform distribution and aggregated distribution have $I_\delta < 1$ and $I_\delta > 1$, respectively, as shown in Fig. 10.

Using the I_δ, the spatial distribution of $Al_{2.7}Fe_{0.3}Ti$ particle in the Al-40vol%$Al_{2.7}Fe_{0.3}Ti$ refiners fabricated under different mixing conditions is quantitatively evaluated. Figure 11 shows the I_δ of these Al-40vol%$Al_{2.7}Fe_{0.3}Ti$ refiners as a function of q. The I_δ of the refiners fabricated without the stearic acid are larger than 1. Therefore, these refiners contain aggregated $Al_{2.7}Fe_{0.3}Ti$ particles. On the other hand, the I_δ of the refiner fabricated with the stearic acid is smaller than 1. These results are not conflict with the microstructural observations shown in Fig. 8. In this way, aggregation of the $Al_{2.7}Fe_{0.3}Ti$ heterogeneous nucleation site particles can be suppressed by the addition of the stearic acid during the mixing.

A defect analysis was carried out on the CT scan of the refiners. The 3D image made semi-transparent to view the location, shape and sizes of the defects are shown in Fig. 12, where the largest voids are colored in red, while the smallest in blue. It is seen that large pores with a size of 0.35 mm^3 can be observed in the refiner fabricated without the

stearic acid, while such large pore cannot be found in the refiner fabricated with the stearic acid. Moreover, only smaller amount of pores are observed in the refiner fabricated with the stearic acid. These results are in good agreement with the relative densities of the refiners measured by Archimedes method shown in Table IV.

Therefore, it is concluded that the refiner with high volume fraction of uniformly dispersed $Al_{2.7}Fe_{0.3}Ti$ heterogeneous nucleation site particles without larger pores can be fabricated by addition of the stearic acid during the preparation of mixing of Al particles and $Al_{2.7}Fe_{0.3}Ti$ particles. It is expected that the grain refiner with uniform distribution of heterogeneous nucleation site particles and without larger pores (refiner fabricated with the stearic acid) should show better grain refining performance comparing with those containing aggregated heterogeneous nucleation site particles and larger pores (refiners fabricated without the stearic acid). In the following, grain refinement performance of Al–40vol%$Al_{2.7}Fe_{0.3}Ti$ refiners fabricated under different mixing conditions will be discussed.

3.4 Grain refinement performance of Al–40 vol%$Al_{2.7}Fe_{0.3}Ti$ refiners fabricated under different mixing conditions

Macrostructures of the Al casts refined by Al-40vol%$Al_{2.7}Fe_{0.3}Ti$ refiners fabricated under mixing time of 10 min, 60 min and 300 min without stearic acid, and 60 min with stearic acid are shown in Figs. 13(a)-13(d), respectively. From left figures to right figures, the holding times are 0 s, 210 s, 600 s, and 1200 s. It is seen that almost fully equiaxed grain structures were obtained in the Al casts using the refine fabricated with stearic acid, as shown in Fig. 13(d).

The average grain size of each Al cast is evaluated and results are plotted against the holding time, as shown in Fig. 14. The minimum grain sizes of Al casts refined by these refiners were 401 μm, 512 μm, 448 μm, and 298 μm, respectively. Acceptable grain refining performance is, now, appeared in the refiner with high volume fraction of heterogeneous nucleation site particles by addition of stearic acid during preparation of mixed powder.

Here, considering about effects of the addition of stearic acid into the grain refiner on its grain refining performance, it is seen from Fig. 14 that the grain refiner with stearic acid has better grain refinement ability than the grain refiner without stearic acid. Now we would like to discuss why the grain refiner fabricated with stearic acid shows better grain refinement ability. One reason is homogeneously distribution of heterogeneous nucleation site particles. As mentioned in Section 3.3, spatial distribution of heterogeneous nucleation site particles in the grain refiner is homogenized by the addition of the stearic acid. Since the nucleation during solidification start on heterogeneous nucleation site particles, it is natural that grain refiner with homogeneously distribution of heterogeneous nucleation site particles have better grain refinement ability. This is because that total surface area of heterogeneous nucleation site particles is larger in isolate distribution of particles rather than aggregately distribution of the particles. Namely, since the formation of a stable nucleus depends on the competition between the driving force for the phase transformation from liquid to solid and the energy required for the formation of a new interface, as shown in Fig. 1, heterogeneous nucleation site particles must be surrounded by Al, which is achieved by isolate distribution of the heterogeneous nucleation site particles. Especially, this tendency would be remarkable in the grain refiner with high volume fraction of heterogeneous nucleation site particles.

Another reason may be the influence of pore and density of the refiners, which could be decreased and increased by addition of the stearic acid, respectively. If a heterogeneous nucleation site particle touches with gas phase, the classical nucleation theory, shown in Figs. 1 and 2, does not hold. To act as heterogeneous nucleation site, the $Al_{2.7}Fe_{0.3}Ti$ particles must be surrounded by molten Al. Although the SPS was carried out under vacuum condition, some retained gas may exist within the pores, which prohibit the grain refining ability. Moreover, the refiners with smaller density tend to buoy up in the molten Al, even though the density of Al-40vol% $Al_{2.7}Fe_{0.3}Ti$ refiner (2.95 $Mg/m^3$for 95% relative density) is larger than that of molten Al (2.391 Mg/m^3 at 660 ^oC [40]). Buoyed up refiner becomes a kind of dross, and the $Al_{2.7}Fe_{0.3}Ti$ particles in the refiner do not act as heterogeneous nucleation site. On the other hand, since the refiner with full density does not buoy up in the molten Al, the $Al_{2.7}Fe_{0.3}Ti$ particles spread into the molten Al effectively, which results in the better grain refining performance. In this way, reducing the pores and aggregation

of heterogeneous nucleation site particles, one can obtain an acceptable refiner with high volume fraction of heterogeneous nucleation site particles.

4. Conclusions

In this study, Al-$Al_{2.7}Fe_{0.3}Ti$ refiners with high volume fraction of the $Al_{2.7}Fe_{0.3}Ti$ heterogeneous nucleation site particles were fabricated by SPS and their grain refining performances for Al cast were investigated. The obtained results are summarized as follows.

1) Refiners with high volume fraction of the $L1_2$-type $Al_{2.7}Fe_{0.3}Ti$ heterogeneous nucleation site particles up to 50vol% can be successfully fabricated by SPS method. However, Al-40vol%$Al_{2.7}Fe_{0.3}Ti$ and Al-50vol%$Al_{2.7}Fe_{0.3}Ti$ refiners have aggregated $Al_{2.7}Fe_{0.3}Ti$ particles and some pores around the aggregated region.
2) The refiners containing the $Al_{2.7}Fe_{0.3}Ti$ particles less than 30vol% shows similar grain refining performance. However, reduced grain refinement performance of refiners containing the $Al_{2.7}Fe_{0.3}Ti$ particles more than 40vol% was found.
3) Spatial distribution analysis of the $Al_{2.7}Fe_{0.3}Ti$ particles in the refiner using Morisita index, I_δ, concluded for Al-40vol%$Al_{2.7}Fe_{0.3}Ti$ refiners fabricated under different mixing conditions shows that addition of adding stearic acid enhances homogeneity of spatial distribution of $Al_{2.7}Fe_{0.3}Ti$ particles. Moreover, only smaller amount of pores are observed in the refiner fabricated with the stearic acid.
4) Acceptable grain refining performance is appeared in the refiner with high volume fraction of heterogeneous nucleation site particles, if the formation of pores and aggregation of the heterogeneous nucleation site particles could be suppressed, which can be achieved by addition of stearic acid during preparation of mixed powder.

Acknowledgments

The authors are thankful for the financial support from The Light Metal Educational Foundation Inc. of Japan and the New Energy and Industrial Technology Development Organization (NEDO) of Japan. This research was also partially supported by the Japan Science and Technology Agency (JST) under Industry-Academia Collaborative R&D Program “Heterogeneous Structure Control: Towards Innovative Development of Metallic

Structural Materials".

References

1) A. Cibula, J. Inst. Met. **76**, 321 (1949-1950).
2) J. A. Marcantonio and L. F. Mondolfo, J. Inst. Met. **98**, 23 (1970).
3) C. D. Mayes, D. G. McCartney, and G. J. Tatlock, Mater. Sci. Eng., A **188**, 283 (1994).
4) M. Easton and D. StJohn, Metall. Mater. Trans. A **30**, 1613 (1999).
5) M. A. Easton and D. H. StJohn, Acta Mater. **49**, 1867 (2001).
6) P. Li., E.G. Kandalova, and V.I. Nikitin, Mater. Lett. **59**, 723 (2005).
7) A. Kamio, Keikinzoku **31**, 136 (1981). [in Japanese].
8) D. Turnbull and B. Vonnegut, Ind. Eng. Chem. **44**, 1292 (1952).
9) B. L. Bramfitt, Metall. Trans. A **1**, 1987 (1970).
10) M. Kato, M. Wada, A. Sato, and T. Mori, Acta Metal. **37**, 749 (1989).
11) M. Kato, Mater. Trans., JIM **33**, 89 (1992).
12) M. Kato, Testu-to-Hagane **78**, 209 (1992) [in Japanese].
13) Y. Watanabe, Q. Zhou, H. Sato, T. Fujii, and T. Inamura, Jpn J. Appl. Phys. **56**, 01AG01 (2017).
14) Y. Watanabe, T. Hamada, and H. Sato, Jpn. J. Appl. Phys. **55**, 01AG01 (2016).
15) Y. Watanabe, T. Hamada, and H. Sato, Jpn. J. Appl. Phys. **56**, 01AG02 (2017).
16) Y. Watanabe, K. Maekawa, and H. Sato, Jpn. J. Appl. Phys. **57**, 01AF08 (2018).
17) Y. Watanabe, R. Yamazaki, K. Yamanaka, and H. Sato, J. Mater. Proc. Tech. **255**, 400 (2018).
18) M. B. Winnicka and R. A. Varin, Scr. Metall. **23**, 1199 (1989).
19) H. Mabuchi, K. Hirukawa, H. Tsuda, and Y. Nakayama, Scr. Metall. Mater. **24**, 505 (1990).
20) Y. Nakayama and H. Mabuchi, Intermetallics **1**, 41 (1993).
21) Y. Watanabe, K. Hirata, and H. Sato, Jpn. J. Appl. Phys. **57**, 01AF04 (2018).
22) Y. J. Wu, R. Kimura, N. Uekawa, K. Kakegawa, and Y. Sasaki, Jpn. J. Appl. Phys. **41**, L219 (2002).
23) A. Kai, N. Johkoh. and T. Miki, Jpn. J. Appl. Phys. **42**, Part 1, 3540 (2003).
24) P. Badica, G. V. Aldica, M. Burdusel, H. Borodianska, Y. Sakka, and O. Vasylkiv, Jpn. J. Appl. Phys. **53**, 05FB22 (2014).
25) Z. Zhang, Y. Watanabe, I. Kim, X. Liu, and X. Bian, Metall. Mater. Trans. A **36**, 837 (2005).
26) Z. Zhang, S. Hosoda, I. S. Kim, and Y. Watanabe, Mater. Sci. Eng. A **425**, 55 (2006).

27) K. X. Wei, P. Liu, W. Wei, Q. B. Du, I. V. Alexandrov, and J. Hu, Appl. Phys. A **122**, 1005 (2016).
28) M. Kawasaki and T. G. Langdon, J. Mater. Sci. **42**, 1782 (2007).
29) K. Suehiro, S. Nishimura, Z. Horita, S. Mitani, K. Takanashi, H. Fujimori, J. Mater. Sci. **43**, 7349 (2008).
30) T. Sakai, H. Miura, A. Goloborodko, and O. Sitdikov, Acta Mater. **57**, 153 (2009).
31) H. Sato, K. Ota, H. Kato, M. Furukawa, M. Azuma, Y. Watanabe, Z.Zhang, and K. Tsuzaki, Mater. Trans. **54**, 1554 (2013).
32) K. L. Bhoite and G. M. Kakandikar, Inter. Eng. Res. J. **2**, 4090 (2015).
33) C. Machio, H. K. Chikwanda, and S. Chikosha, J. South. Afric. Inst. Min. Met. **111**, 149 (2011).
34) M. Ramezani and T. Neitzert, J. Achiev. Mater. Manuf. Eng. **55**, 790 (2012).
35) M. Morisita, Mem. Fac. Sci. Kyushu Univ., E **2**, 215 (1959).
36) M. Morisita, Res. Popul. Ecol. **4**, 1 (1962).
37) M. Morisita, Res. Popul. Ecol. **13**, 1 (1971).
38) M. Kubota, Keikinzoku **67**, 243 (2017). [in Japanese].
39) L. Zhang and X. Guo, Mater. Trans. **59**, 528 (2018).
40) M. Leitner, T. Leitner, A. Schmon, K. Aziz and G. Pottlacher, Metall. Mater. Trans. A **48**, 3036 (2017).

Table Captions

Table. I. Casting conditions using Al-$Al_{2.7}Fe_{0.3}Ti$ refiners.

Table. II. Compositional analysis of Al-5vol%$Al_{2.7}Fe_{0.3}Ti$ refiner shown in Fig. 4(a') [mol%].

Table. III. Relative densities of fabricated Al-$Al_{2.7}Fe_{0.3}Ti$ refiners measured by Archimedes method.

Table IV. Relative density results by Archimedes method.

Figure Captions

Fig. 1. (Color online) Schematic representation showing the formation of a spherical segment nucleus of crystal on the substrate, *i.e.*, heterogeneous nucleation site. Where θ is the wetting angle, γ_{LC}, γ_{CS} and γ_{LS} are interface free energies per unit area between liquid and crystal, between crystal and substrate, and between liquid and substrate, respectively.

Fig. 2. (Color online) The $\{(2+\cos\theta)(1-\cos\theta)^2\}/4$ value in eq. (4) as a function of wetting angle, θ.

Fig. 3. (Color online) Flow diagram of experimental procedure.

Fig. 4. (Color online) SEM microstructure photographs of Al-$Al_{2.7}Fe_{0.3}Ti$ refiners. (a) and (a') Al-5vol%$Al_{2.7}Fe_{0.3}Ti$, (b) and (b') Al-10vol%$Al_{2.7}Fe_{0.3}Ti$, (c) and (c') Al-20vol%$Al_{2.7}Fe_{0.3}Ti$, (d) and (d') Al-30 vol%$Al_{2.7}Fe_{0.3}Ti$, (e) and (e') Al-40vol%$Al_{2.7}Fe_{0.3}Ti$, and (f) and (f') Al-50vol%$Al_{2.7}Fe_{0.3}Ti$ refiners.

Fig. 5. (Color online) XRD result of Al-$Al_{2.7}Fe_{0.3}Ti$ refiners: (a) Al-5vol%$Al_{2.7}Fe_{0.3}Ti$, (b) Al-10vol%$Al_{2.7}Fe_{0.3}Ti$, (c) Al-20 vol%$Al_{2.7}Fe_{0.3}Ti$, (d) Al-30vol%$Al_{2.7}Fe_{0.3}Ti$, (e) Al-40vol% $Al_{2.7}Fe_{0.3}Ti$, and (f) Al-50vol%$Al_{2.7}Fe_{0.3}Ti$ refiners.

Fig. 6. Macrographs of Al castings refined by (a) Al-5vol%$Al_{2.7}Fe_{0.3}Ti$, (b) Al-10vol%$Al_{2.7}Fe_{0.3}Ti$, (c) Al-20vol%$Al_{2.7}Fe_{0.3}Ti$, (d) Al-30vol%$Al_{2.7}Fe_{0.3}Ti$, (e) Al-40vol%$Al_{2.7}Fe_{0.3}Ti$, and (f) Al-50vol%$Al_{2.7}Fe_{0.3}Ti$ refiners. (g) Unrefined Al cast.

Fig. 7. (Color online) Mean grain size of Al casts refined by Al-$Al_{2.7}Fe_{0.3}Ti$ refiners with different volume fraction of $Al_{2.7}Fe_{0.3}Ti$ heterogeneous nucleation site particles plotted against holding time.

Fig. 8. SEM microstructure photographs of Al-40 vol%$Al_{2.7}Fe_{0.3}Ti$ refiners fabricated without stearic acid at mixing time of (a)10 min, (b) 60 min, (c) 300 min and (d) with stearic acid at stirring time of 60 min.

Fig. 9. (Color online) Typical particle distributions. (a) Poisson's distribution, (b) uniform distribution, and (c) aggregated distribution.

Fig. 10. (Color online) I_δ of (a) Poisson's distribution, (b) uniform distribution, and (c) aggregated distribution, as a function of q.

Fig. 11. (Color online) I_δ of Al-40 vol%$Al_{2.7}Fe_{0.3}Ti$ refiners fabricated under different mixing conditions as a function of q.

Fig. 12. (Color online) Defect analysis indicating the location, shape and size of each defect of Al-40 vol%$Al_{2.7}Fe_{0.3}Ti$ refiners fabricated without stearic acid at mixing time of (a)10 min, (b) 60 min, (c) 300 min and (d) with stearic acid at stirring time of 60 min.

Fig. 13. Macrographs of Al castings refined by the Al-40 vol%$Al_{2.7}Fe_{0.3}Ti$ refiners fabricated without stearic acid at stirring time of (a)10 min, (b) 60 min, (c) 300 min and (d) with stearic acid at stirring time of 60 min.

Fig. 14. (Color online) Mean grain size of Al cast refined by the Al-40vol%$Al_{2.7}Fe_{0.3}Ti$ refiners fabricated under different mixing conditions.

Table. I. Casting conditions using Al-$Al_{2.7}Fe_{0.3}Ti$ refiners.

Refiner	Amount of molten Al [g]	Addition of refiner [g]	Amount of $Al_{2.7}Fe_{0.3}Ti$ in cast [g]
Al-5vol%$Al_{2.7}Fe_{0.3}Ti$	147.64	2.36	0.16
Al-10vol%$Al_{2.7}Fe_{0.3}Ti$	148.80	1.20	
Al-20vol%$Al_{2.7}Fe_{0.3}Ti$	149.38	0.62	
Al-30vol%$Al_{2.7}Fe_{0.3}Ti$	149.58	0.42	
Al-40vol%$Al_{2.7}Fe_{0.3}Ti$	149.67	0.33	
Al-50vol%$Al_{2.7}Fe_{0.3}Ti$	149.73	0.27	

Table. II. Compositional analysis of Al-5vol%$Al_{2.7}Fe_{0.3}Ti$ refiner shown in Fig. 4(a') [mol%].

		Al	Ti	Fe
1	(Al matrix)	99.9	0.0	0.1
2	($Al_{2.7}Fe_{0.3}Ti$)	63.1	27.6	8.3
3	(Fe-rich second phase)	63.0	22.2	14.8

Table. III. Relative densities of fabricated Al-$Al_{2.7}Fe_{0.3}Ti$ refiners measured by Archimedes method.

Refiner	Relative density [%]
Al-5 vol%$Al_{2.7}Fe_{0.3}Ti$	97.99
Al-10 vol%$Al_{2.7}Fe_{0.3}Ti$	97.76
Al-20 vol%$Al_{2.7}Fe_{0.3}Ti$	97.86
Al-30 vol%$Al_{2.7}Fe_{0.3}Ti$	96.85
Al-40 vol%$Al_{2.7}Fe_{0.3}Ti$	94.70
Al-50 vol%$Al_{2.7}Fe_{0.3}Ti$	94.33

Table IV. Relative density results by Archimedes method.

Refiner	Stearic Acid	Mixing Time [min]	Relative Density [%]
Al-40 vol%$Al_{2.7}Fe_{0.3}Ti$	w/o	10	94.93
		60	94.70
		300	95.04
	w/	60	96.44

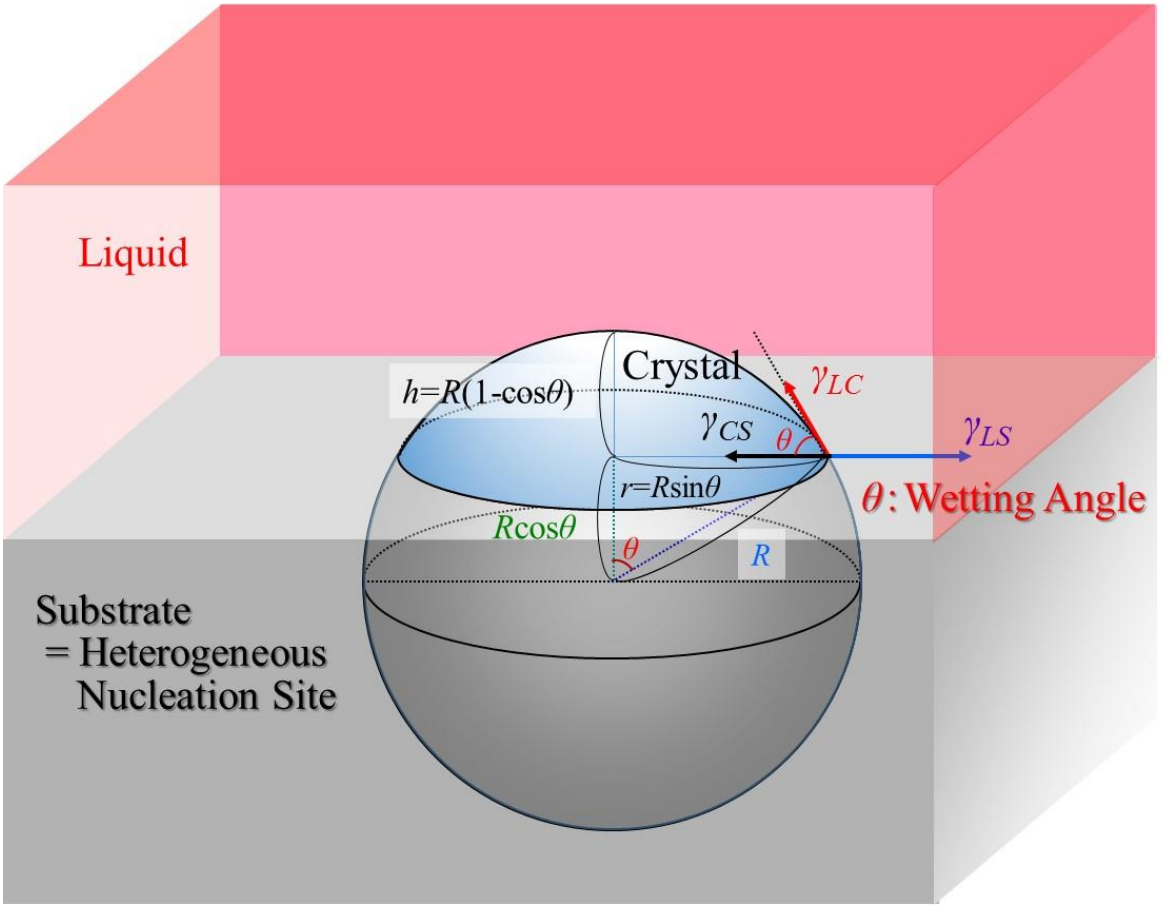

Fig. 1. (Color online) Schematic representation showing the formation of a spherical segment nucleus of crystal on the substrate, *i.e.*, heterogeneous nucleation site. Where θ is the wetting angle, γ_{LC}, γ_{CS} and γ_{LS} are interface free energies per unit area between liquid and crystal, between crystal and substrate, and between liquid and substrate, respectively.

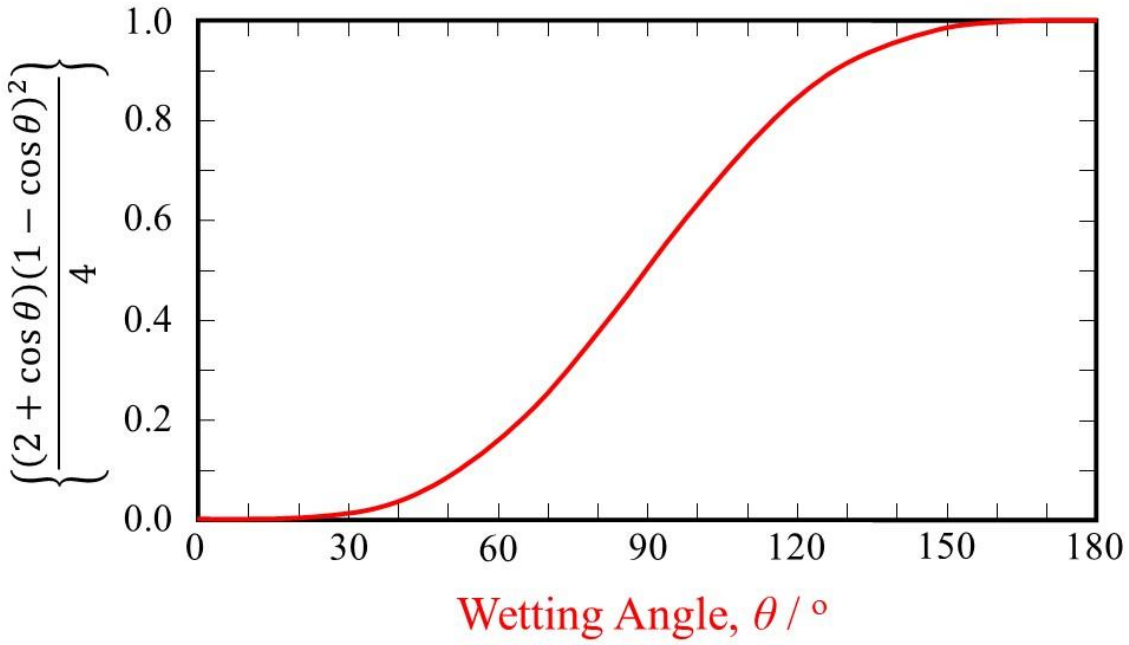

Fig. 2. (Color online) The $\{(2+\cos\theta)(1-\cos\theta)^2\}/4$ value in eq. (4) as a function of wetting angle, θ.

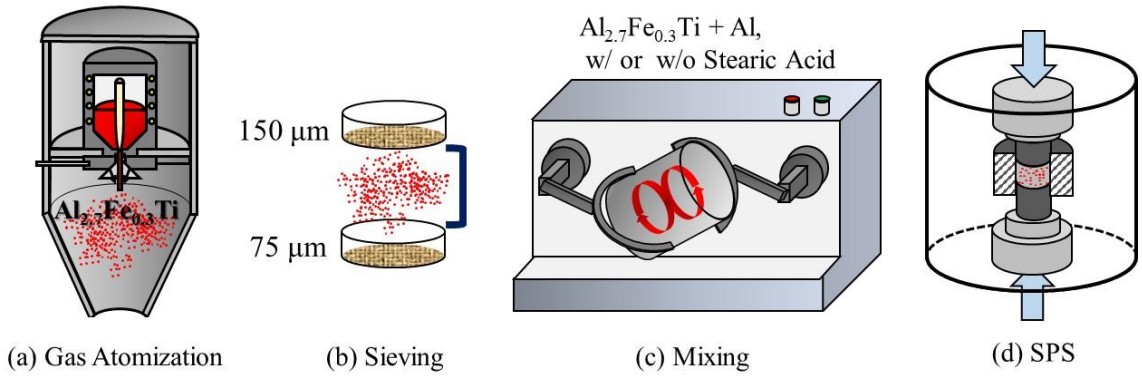

Fig. 3. (Color online) Flow diagram of experimental procedure.

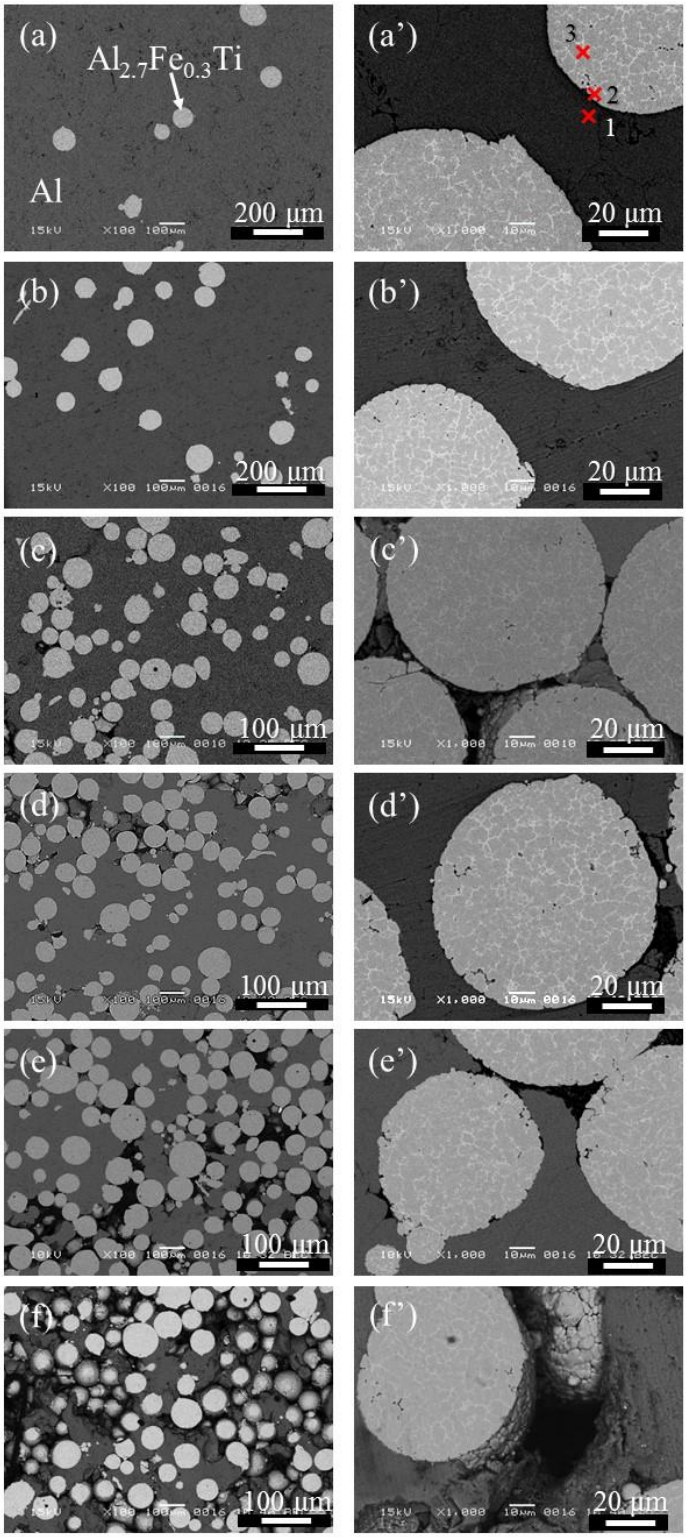

Fig. 4. (Color online) SEM microstructure photographs of Al-$Al_{2.7}Fe_{0.3}Ti$ refiners. (a) and (a') Al-5vol%$Al_{2.7}Fe_{0.3}Ti$, (b) and (b') Al-10vol%$Al_{2.7}Fe_{0.3}Ti$, (c) and (c') Al-20vol%$Al_{2.7}Fe_{0.3}Ti$, (d) and (d') Al-30 vol%$Al_{2.7}Fe_{0.3}Ti$, (e) and (e') Al-40vol%$Al_{2.7}Fe_{0.3}Ti$, and (f) and (f') Al-50vol%$Al_{2.7}Fe_{0.3}Ti$ refiners.

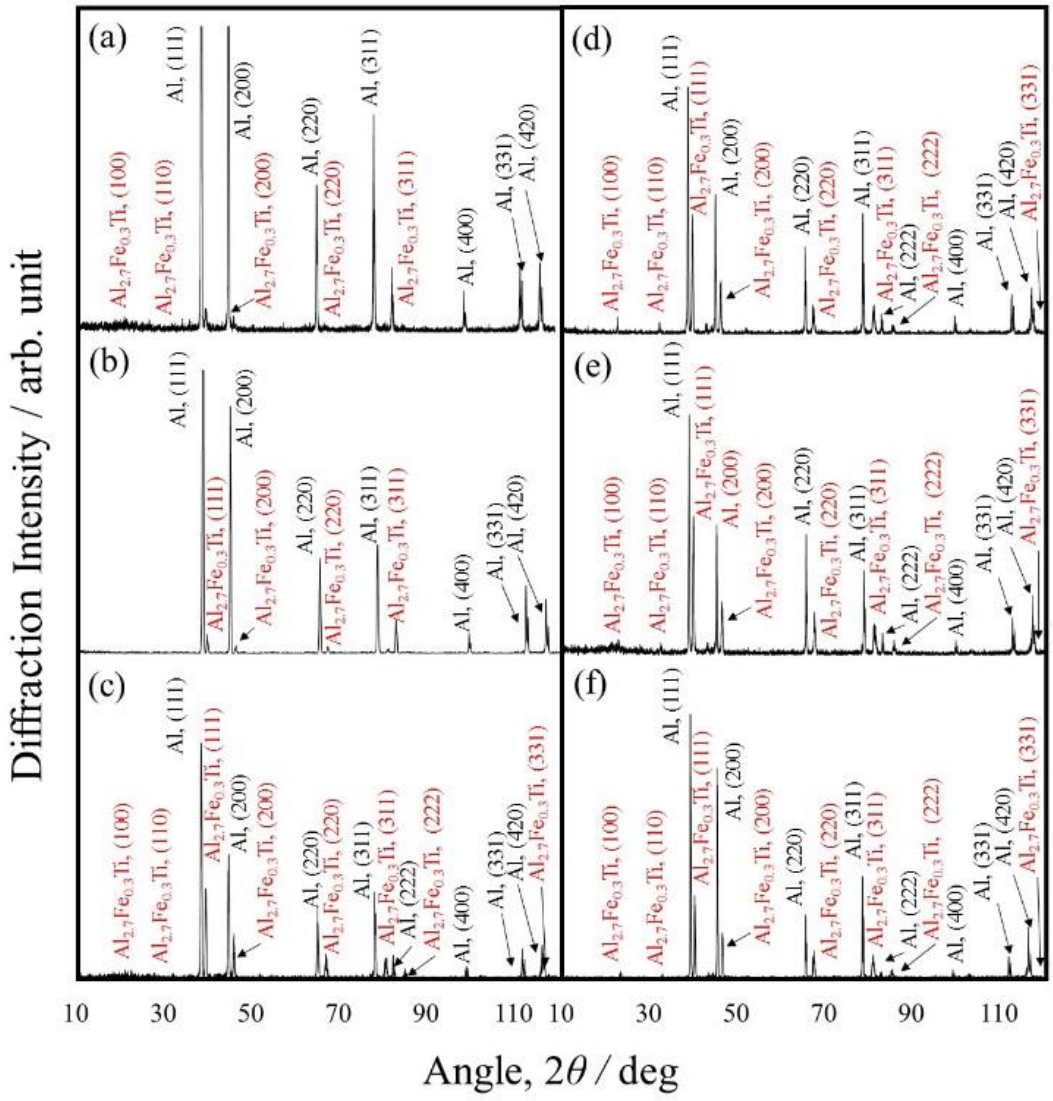

Fig. 5. (Color online) XRD result of Al-$Al_{2.7}Fe_{0.3}Ti$ refiners: (a) Al-5vol%$Al_{2.7}Fe_{0.3}Ti$, (b) Al-10vol%$Al_{2.7}Fe_{0.3}Ti$, (c) Al-20 vol%$Al_{2.7}Fe_{0.3}Ti$, (d) Al-30vol%$Al_{2.7}Fe_{0.3}Ti$, (e) Al-40vol% $Al_{2.7}Fe_{0.3}Ti$, and (f) Al-50vol%$Al_{2.7}Fe_{0.3}Ti$ refiners.

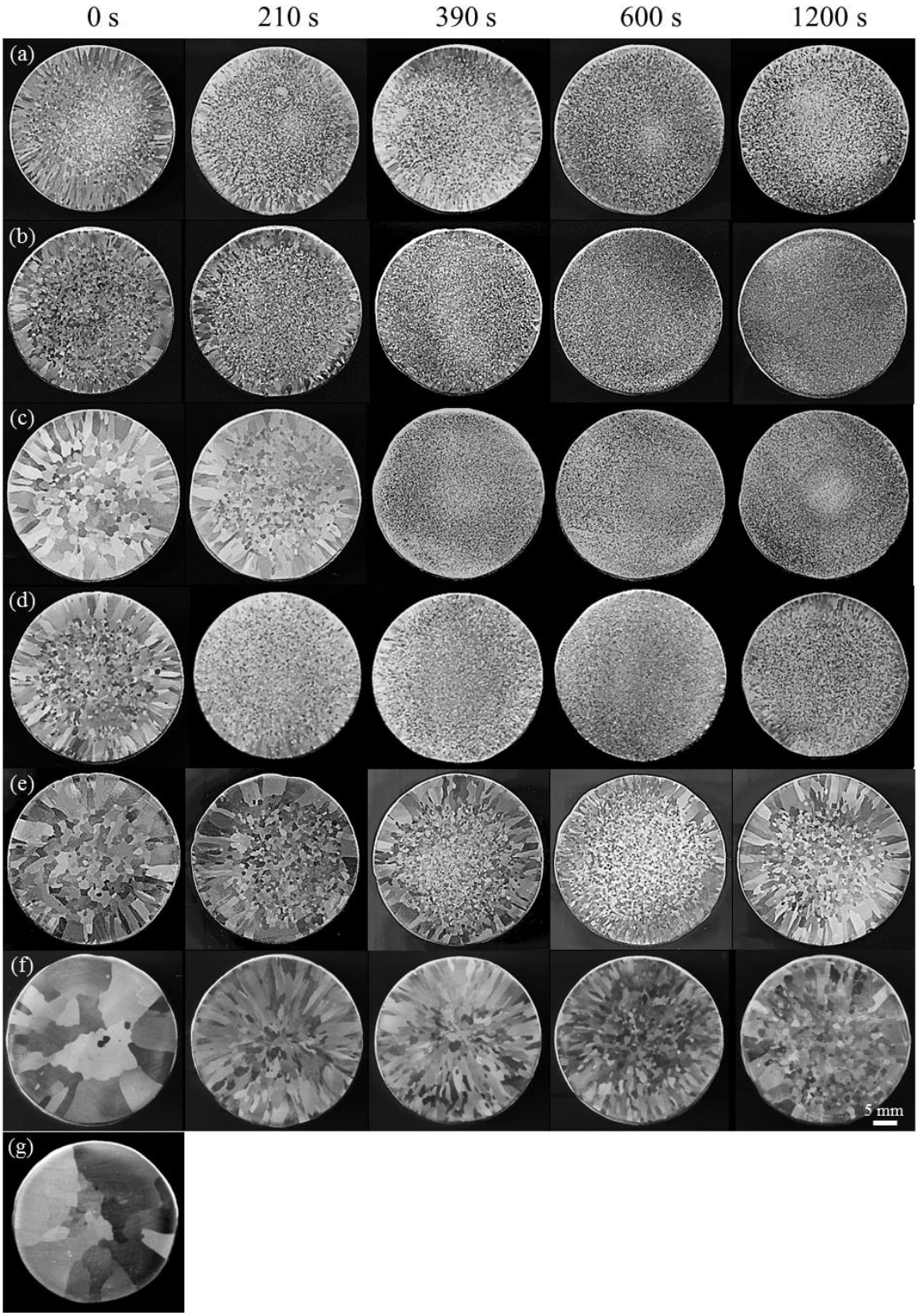

Fig. 6. Macrographs of Al castings refined by (a) Al-5vol%$Al_{2.7}Fe_{0.3}Ti$, (b) Al-10vol%$Al_{2.7}Fe_{0.3}Ti$, (c) Al-20vol%$Al_{2.7}Fe_{0.3}Ti$, (d) Al-30vol%$Al_{2.7}Fe_{0.3}Ti$, (e) Al-40vol%$Al_{2.7}Fe_{0.3}Ti$, and (f) Al-50vol%$Al_{2.7}Fe_{0.3}Ti$ refiners. (g) Unrefined Al cast.

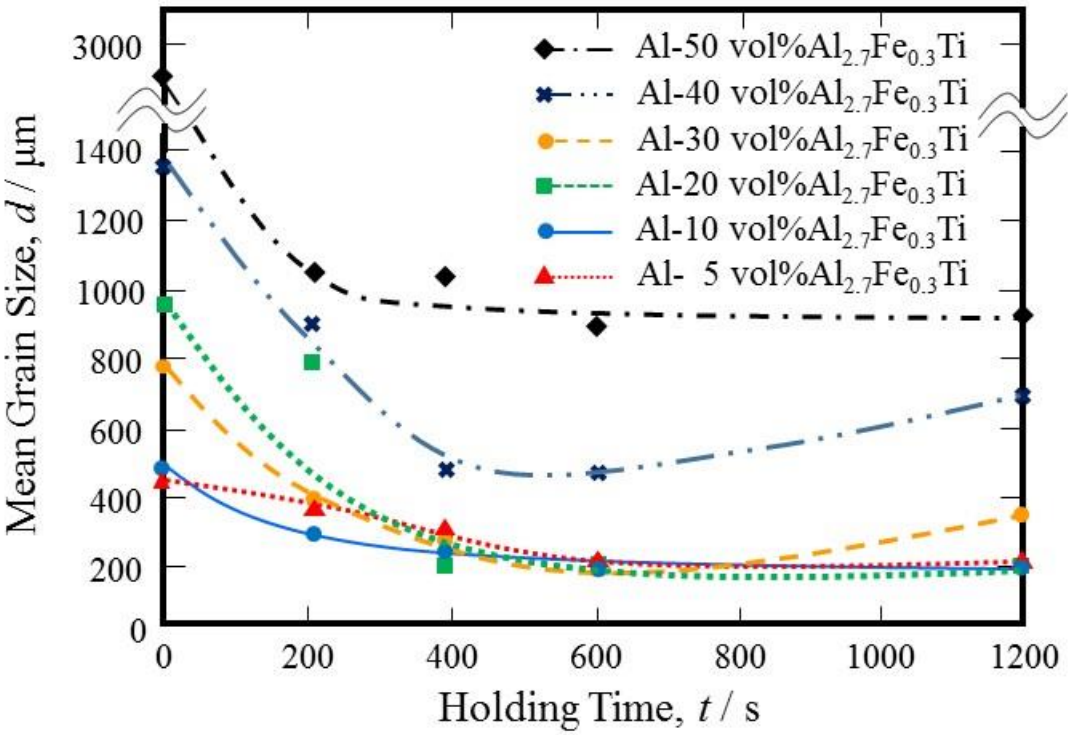

Fig. 7. (Color online) Mean grain size of Al casts refined by Al-$Al_{2.7}Fe_{0.3}Ti$ refiners with different volume fraction of $Al_{2.7}Fe_{0.3}Ti$ heterogeneous nucleation site particles plotted against holding time.

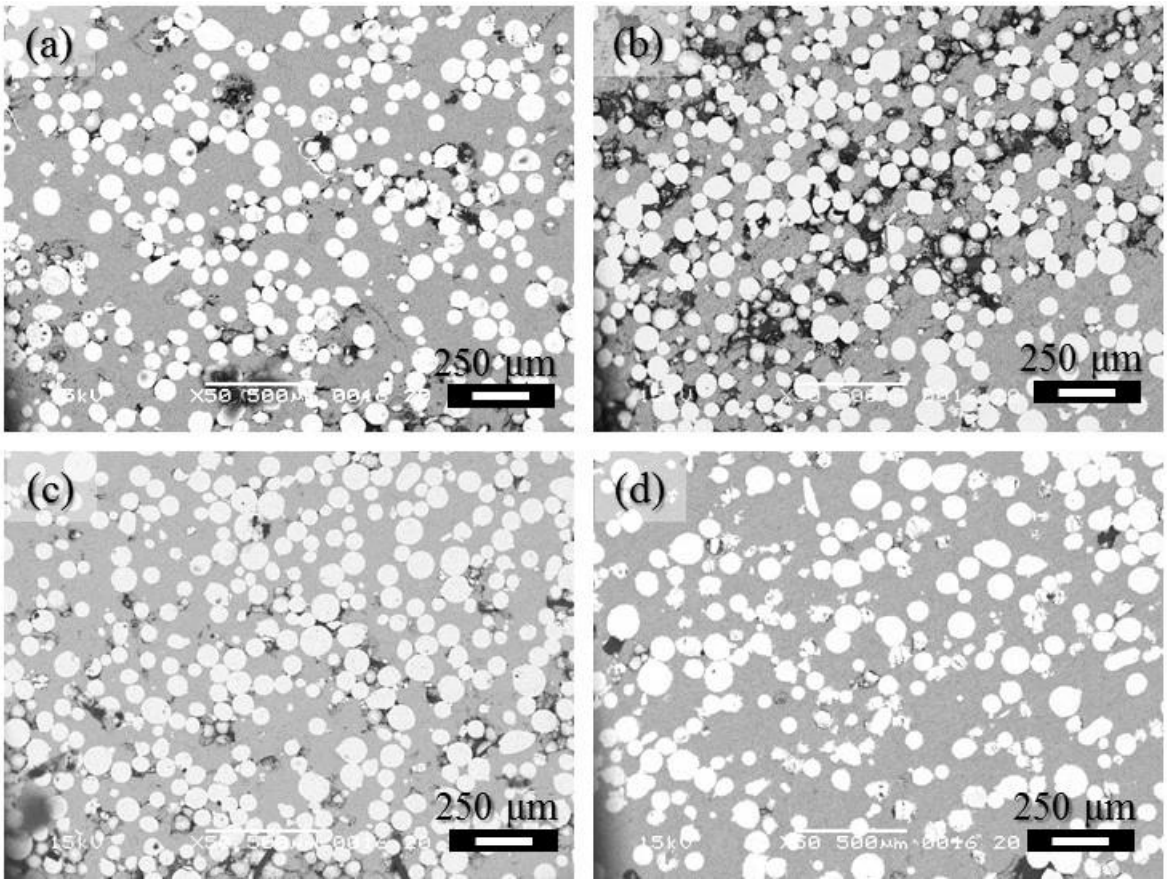

Fig. 8. SEM microstructure photographs of Al-40 vol%$Al_{2.7}Fe_{0.3}Ti$ refiners fabricated without stearic acid at mixing time of (a)10 min, (b) 60 min, (c) 300 min and (d) with stearic acid at stirring time of 60 min.

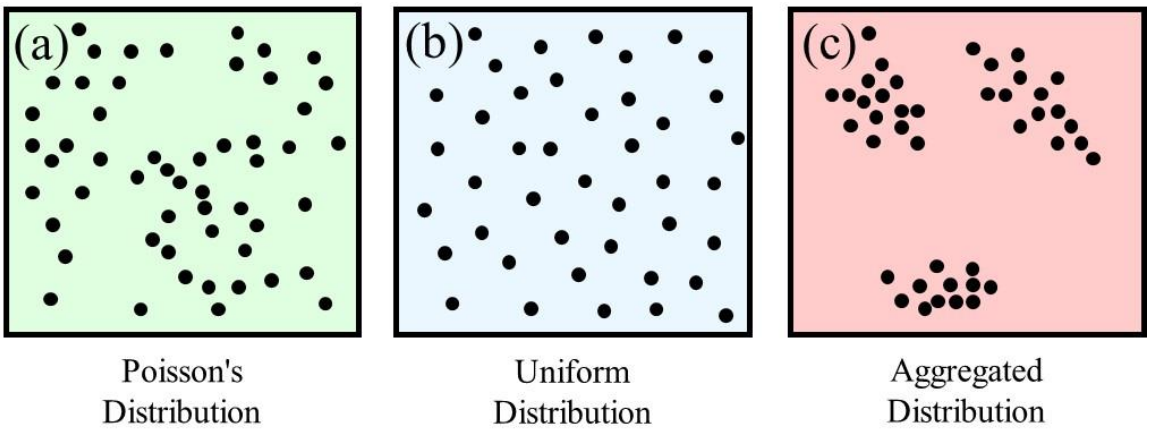

Fig. 9. (Color online) Typical particle distributions. (a) Poisson's distribution, (b) uniform distribution, and (c) aggregated distribution.

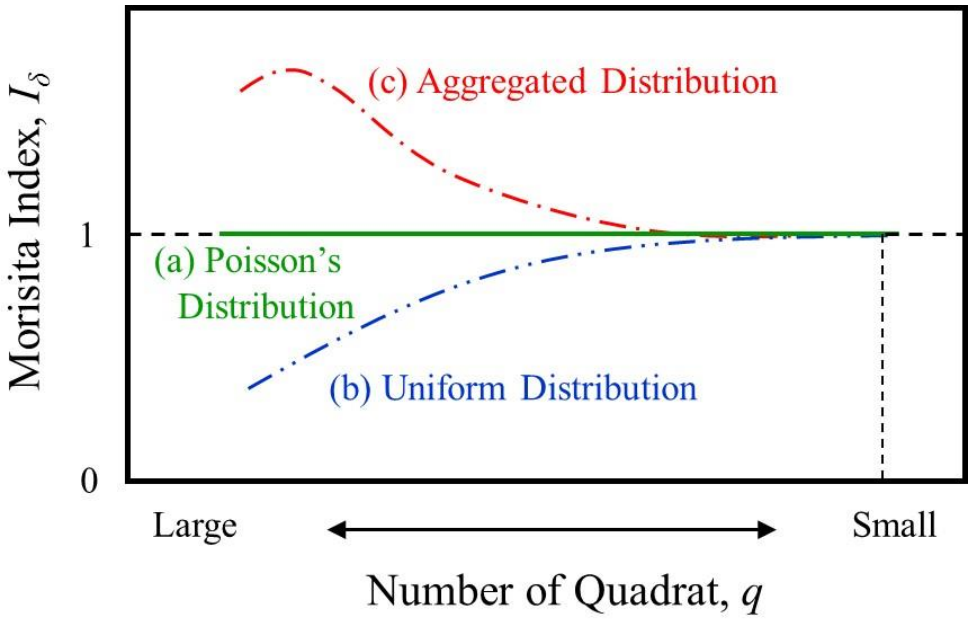

Fig. 10. (Color online) Morisita Index, I_δ, of (a) Poisson's distribution, (b) uniform distribution, and (c) aggregated distribution, as a function of q.

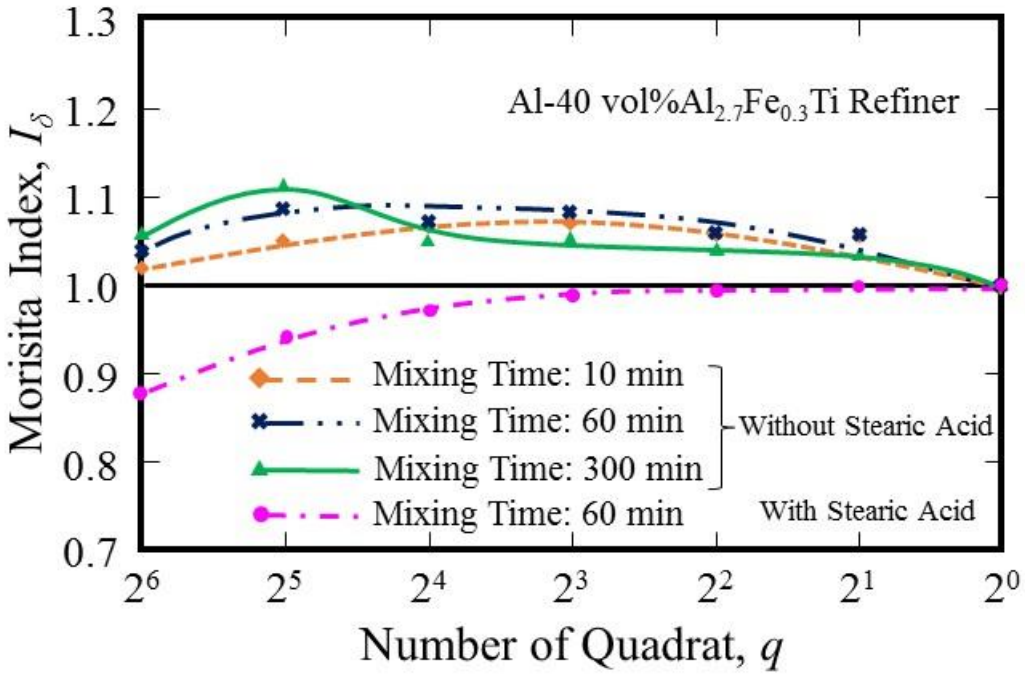

Fig. 11. (Color online) Morisita Index of Al-40 vol%$Al_{2.7}Fe_{0.3}Ti$ refiners fabricated under different mixing conditions as a function of q.

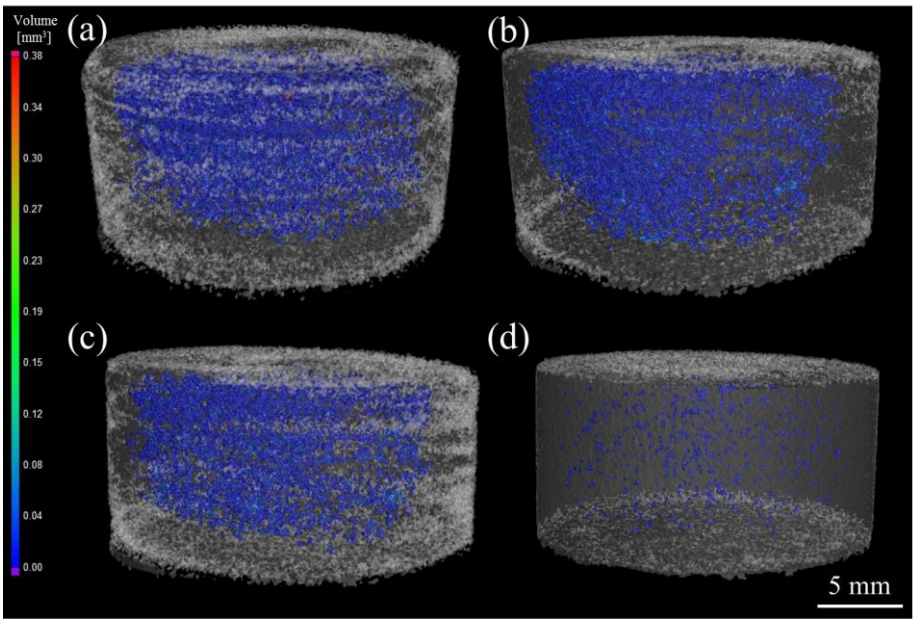

Fig. 12. (Color online) Defect analysis indicating the location, shape and size of each defect of Al-40 vol%$Al_{2.7}Fe_{0.3}Ti$ refiners fabricated without stearic acid at mixing time of (a)10 min, (b) 60 min, (c) 300 min and (d) with stearic acid at stirring time of 60 min.

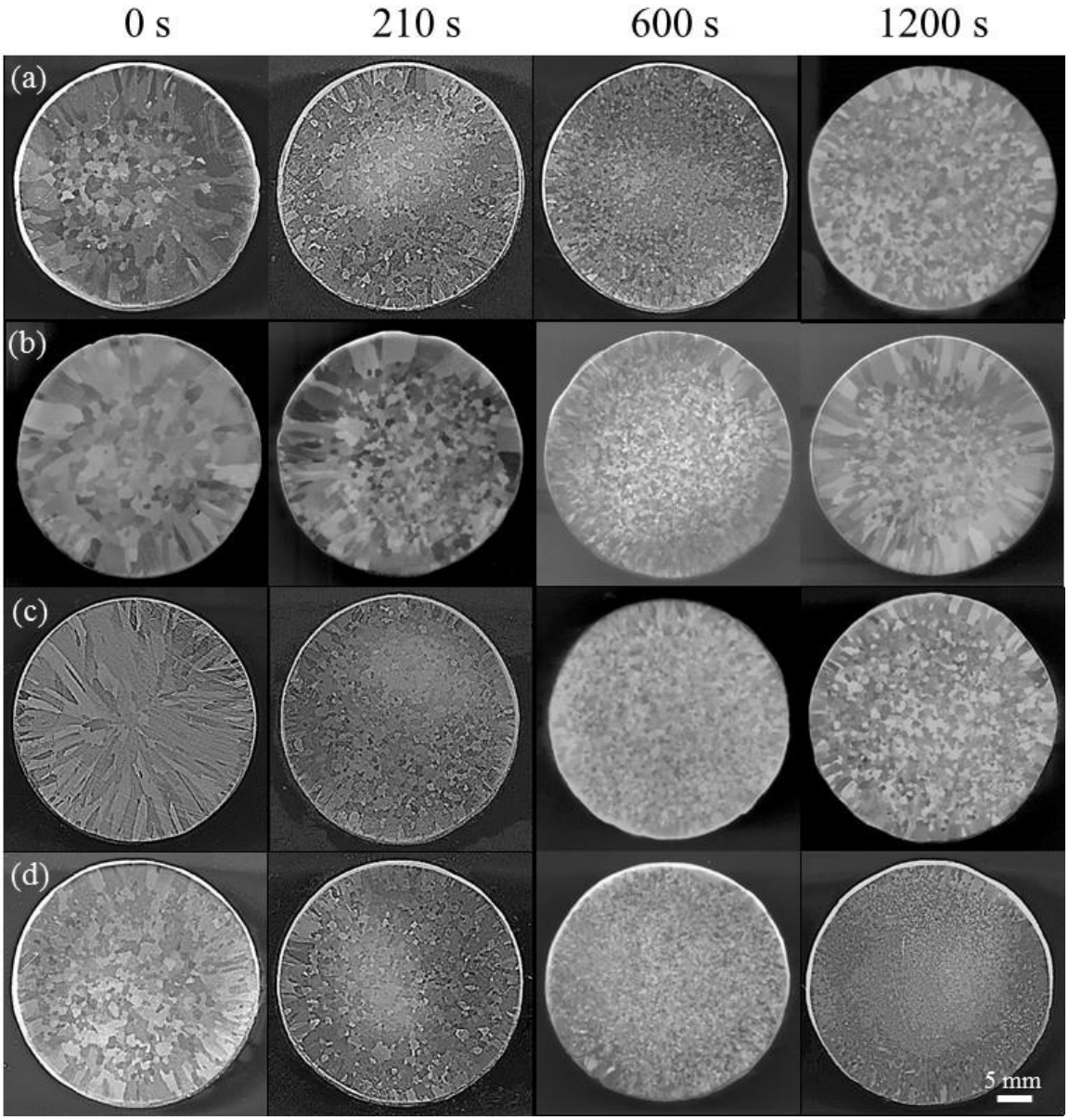

Fig. 13. Macrographs of Al castings refined by the Al-40 vol%$Al_{2.7}Fe_{0.3}Ti$ refiners fabricated without stearic acid at stirring time of (a)10 min, (b) 60 min, (c) 300 min and (d) with stearic acid at stirring time of 60 min.

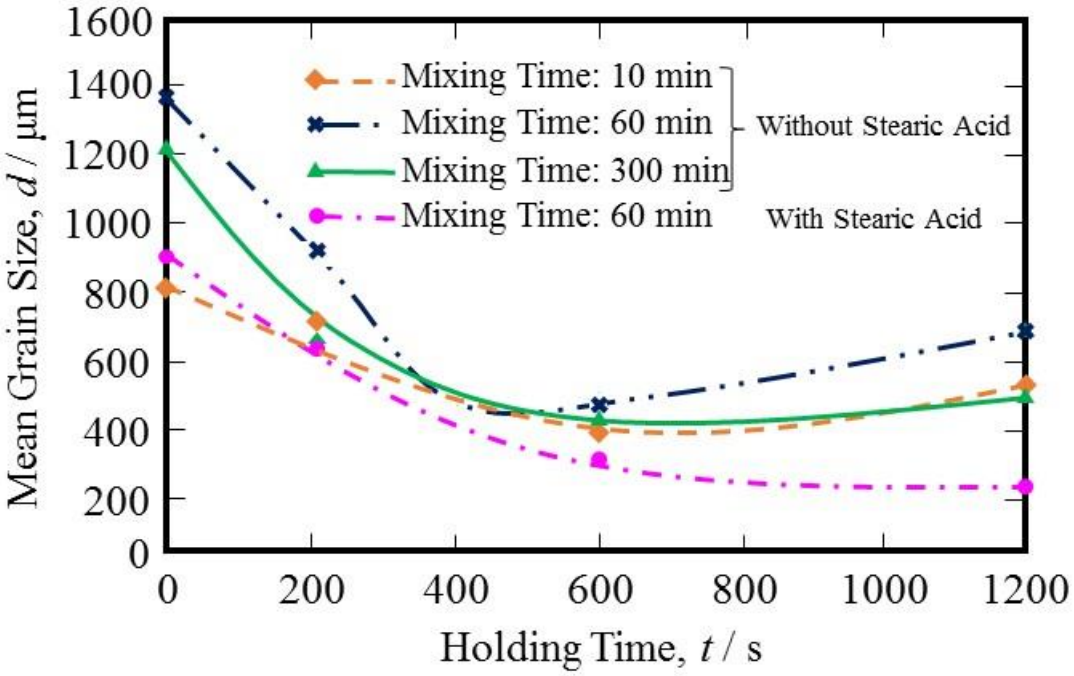

Fig. 14. (Color online) Mean grain size of Al cast refined by the Al-40vol%$Al_{2.7}Fe_{0.3}Ti$ refiners fabricated under different mixing conditions.